Eur. Phys. J. Special Topics **226**, 3113–3128 (2017)

DOI: 10.1140/epjst/e2017-70081-3

THE EUROPEAN PHYSICAL JOURNAL SPECIAL TOPICS

Review

Anomalous transport in heterogeneous media

Jürgen Horbach[1,a], Nima H. Siboni[1], and Simon K. Schnyder[1,2]

[1] Institut für Theoretische Physik II, Heinrich-Heine-Universität Düsseldorf, Universitätsstraße 1, 40225 Düsseldorf, Germany
[2] Fukui Institute for Fundamental Chemistry, Kyoto University, Kyoto 606–8103, Japan

Received 28 April 2017 / Received in final form 1 June 2017
Published online 10 August 2017

Abstract. The diffusion dynamics of particles in heterogeneous media is studied using particle-based simulation techniques. A special focus is placed on systems where the transport of particles at long times exhibits anomalies such as subdiffusive or superdiffusive behavior. First, a two-dimensional model system is considered containing gas particles (tracers) that diffuse through a random arrangement of pinned, disk-shaped particles. This system is similar to a classical Lorentz gas. However, different from the original Lorentz model, soft instead of hard interactions are considered and we also discuss the case where the tracer particles interact with each other. We show that the modification from hard to soft interactions strongly affects anomalous-diffusive transport at high obstacle densities. Second, non-linear active micro-rheology in a glass-forming binary Yukawa mixture is investigated, pulling single particles through a deeply supercooled state by applying a constant force. Here, we observe superdiffusion in force direction and analyze its origin. Finally, we consider the Brownian dynamics of a particle which is pulled through a two-dimensional random force field. We discuss the similarities of this model with the Lorentz gas as well as active micro-rheology in glass-forming systems.

1 Introduction

The transport of particles through frozen or quasi-frozen host structures is ubiquitous in many condensed matter systems. Examples are the protein motion through crowded cells [1–3], the flow and diffusion of gas molecules through porous media [4] and the driven motion of tracer particles through supercooled liquids or glasses [5]. Especially for disordered host structures, one often encounters anomalous transport phenomena, as indicated by a subdiffusive or superdiffusive motion on intermediate time scales or even asymptotically in the long-time limit. The origin of anomalous transport is often not well understood on a microscopic level, except for cases where the transport properties fall into a universality class and thus can be accurately studied in terms of simple minimal models [6], analogous to the critical behavior of Ising models in the framework of the theory of phase transitions. In this review, we present computer simulation studies of different systems, associated with molecular

[a] e-mail: horbach@thphy.uni-duesseldorf.de

transport through heterogeneous media. A special focus is placed on the question to what extent anomalous transport phenomena in these systems are universal and can be understood in terms of minimal models or theoretical approaches such as mode coupling theory [7].

Section 2 is on dilute soft-sphere fluids confined in a random arrangement of pinned particles that serve as obstacles for the motion of the fluid particles. This system is similar to the classical Lorentz gas [8], with the modification of soft instead of hard interactions between the fluid particles and the obstacles, and we also consider the case where the fluid particles interact with each other. We show that especially the modification to soft interactions has consequences on the transport properties at high obstacle density. Upon increasing the obstacle density, the original Lorentz gas exhibits a transition towards a localization of the fluid particles. This transition happens at a critical density, associated with the percolation transition of the void space, provided for the motion of the fluid particles. At the transition, the fluid particles move through the fractal structure of the void space and, as a consequence, the diffusive motion becomes anomalous. We observe that in the modified Lorentz model with soft interactions this transition is in general rounded. Anomalous diffusion is still observed, but it is reflected in effective regimes of subdiffusive behavior on intermediate time scales, different from the original Lorentz gas where at the transition a non-linear, subdiffusive growth of the mean-squared displacement with a universal exponent is seen in the long-time limit.

In Section 3, a binary glass-forming fluid in its deeply supercooled state is simulated, applying a technique that in the context of bio- and soft matter systems is known as active micro-rheology [5]. To this end, single particles are driven through the system by the application of a constant force. In this manner, a time-scale separation between the motion of the pulled particle and the surrounding supercooled "host matrix" is achieved and the pulled particle probes the local viscoelastic properties of the host fluid. A striking observation in our system is the occurrence of superdiffusion of the pulled particle in force direction which is connected to a broad waiting time distribution in the cages of the host fluid.

The system that we consider in Section 4 shares similarities with those of the two previous sections. Here, a Langevin equation for a particle pulled through a two-dimensional quenched random force landscape is solved. In one dimensions this model is well understood and has been extensively studied by Bouchaud et al. [9,10], displaying a very rich phase behavior with a creeping as well as a superdiffusive regime, the latter with similar features as those found for active micro-rheology in glass-forming fluids. Here, we study the two-dimensional version of the Bouchaud model in order to see to what extent anomalous transport properties such as superdiffusion in the long-time limit are also seen in two dimensions and not just a special feature due to the restriction to one spatial dimension.

2 Two-dimensional fluids with randomly pinned particles

2.1 Partly pinned fluid systems

Recently, there have been numerous attempts to shed light on the nature of the structural glass transition by studying glass-forming systems where a fraction of particles is pinned [11–16]. Either the pinned particles form a wall with a similar disordered structure ("amorphous boundary conditions" [11]) or a fraction of particles in the bulk system is randomly selected and fixed in space. However, as has been nicely shown by Krakoviack [17,18] for the latter partly pinned systems, the pinning process does not only couple to the glassy properties of the system under consideration. Already for normal fluids, i.e., fluids without any glassy properties, thermodynamics

and transport properties are strongly affected by the pinning process and thus for glassy systems these effects interfere with those due to structural relaxation in the corresponding unpinned bulk systems. Furthermore, also in systems with amorphous boundary conditions, the free energy of the system is different from the corresponding one with periodic boundary conditions, as has been shown in terms of a simple argument by Cavagna et al. [11] and via thermodynamic integration techniques in a simulation study of a glass-forming binary Lennard-Jones mixture [19].

As a paradigm for a system with quenched disorder, the classical Lorentz gas has been investigated by Götze et al. [20–22] in the framework of a mode-coupling theory which has been shown to be equivalent to a self-consistent kinetic ring theory [23]. Krakoviack has proposed a mode-coupling theory for partly pinned fluids [24,25]. As shown in these works, depending on the density of the fluid and concentration of pinning sites, there is a competition between diffusion-localization transitions and the "usual" glass transition. The former transition occurs in a regime of low fluid densities and is similar to the delocalization-to-localization transition in the classical Lorentz gas [8], as described in the Introduction.

Here, we consider two-dimensional modified versions of the Lorentz gas where, in particular, instead of hard disks, soft obstacle particles are considered. In Section 2.2, we describe a recent experimental realization of a soft Lorentz gas in terms of a colloidal system. Then, Section 2.3 is devoted to a simulation study of a similar system that demonstrates that the Lorentz gas with soft interactions is significantly different from its counterpart with hard interactions in that the boundaries of the accessible void space are smeared out and therefore, the percolation network of the system with hard interactions is replaced by a potential energy landscape with finite barriers between the pores.

2.2 Experimental realization

Two-dimensional colloidal fluids can be realized by sedimenting colloidal particles onto a glass plate. Thorneywork et al. [26–29] have used such a quasi-two-dimensional setup with colloidal hard sphere particles and showed that the radial distribution function is in quantitative agreement with density functional theory and Monte Carlo simulations of corresponding hard-disk fluids [26,27]. This also holds for the long-time self-diffusion constant where the colloidal experiment is in quantitative agreement with Brownian dynamics simulations, provided that the self-diffusion constant at a given area fraction Φ of the colloids is scaled by the self-diffusion constant at infinite dilution [27]. Since in Brownian dynamics simulations hydrodynamic interactions are not taken into account, the agreement of the long-time self-diffusion constants indicates that they do not affect the long-time diffusion of the colloidal hard-sphere fluid in a quasi-two-dimensional geometry.

A colloidal realization of a Lorentz gas model has been presented by Skinner et al. [30,31]. Here, a slightly size-disparate mixture of superparamagnetic colloidal spheres is used. This system is confined between two glass slides such that the larger particles, forming the obstacle matrix, are immobilized while the smaller ones, the fluid particles, are free to move. In the absence of a magnetic field the particles interact with each other like hard spheres. By applying an external magnetic field B perpendicular to the plane of motion, a soft-repulsive pair interaction between the superparamagnetic particles proportional to B^2/r^3 (with r the distance between two particles) is induced. Thus, by varying the strength of the magnetic field, the area fractions of the fluid and matrix particles can be controlled *in situ* without changing the matrix configuration.

The main findings of the experiments by Skinner et al. [30,31] can be summarized as follows: With increasing area fraction of the matrix the fluid particles exhibit a

crossover from delocalized to localized motion. In the delocalized regime, the dynamics is always diffusive at long times and subdiffusive at intermediate times, provided that the matrix area fraction is sufficiently high. In the localized regime, the fluid particles are trapped in finite pockets. This behavior is reminiscent of the delocalization-to-localization transition in the hard-disk Lorentz gas. However, this is not anymore a sharp transition at a critical density but it is instead rounded due to the soft-repulsive matrix-fluid interactions. The mechanism of this rounding has been elucidated by simulations, presented in the next section.

2.3 Rounded localization transitions in model porous media

In the original Lorentz gas, hard interactions between the fluid particle and the obstacles are assumed and therefore, the obstacles can be seen as infinite "energy barriers" for the motion of the tracer particle. At the percolation transition of the void space, the structure of the void space is fractal and the diffusion of the fluid particle through this fractal structure leads to anomalous diffusion in the long-time limit. This behavior can be directly seen in the mean-squared displacement (MSD) of the tracer particle, $\delta r^2(t) = \langle(\mathbf{r}_\mathrm{F}(t) - \mathbf{r}_\mathrm{F}(0))^2\rangle$ (with $\mathbf{r}_\mathrm{F}(t)$ the position of fluid particle at time t and the angled brackets being an ensemble average). It grows asymptotically as $\delta r^2(t) \sim t^{2/z}$, where z is a universal dynamic exponent that has the value $z \approx 2/3.036$ in the two-dimensional case [32].

If one generalizes the Lorentz model by introducing soft instead of hard interactions, the void space that the fluid particle effectively sees depends on its energy. Energy barriers due to the obstacles are no longer infinite and thus small channels in the void space that are impervious for fluid particles with a given energy might be pervious for a fluid particle with a slightly higher energy. As a consequence, the location of the percolation transition in a soft Lorentz model depends on the energy of the tracer particle (which is conserved assuming Newtonian dynamics for its equation of motion). Moreover, for the case of an ideal gas in a disordered arrangement of soft obstacles, each fluid particle sees a percolation transition of the void space at a different obstacle density and, as we demonstrate below, the transition from a delocalized to a localized motion of the fluid particles is rounded.

Molecular dynamics simulations are performed for a two-dimensional soft-sphere Lorentz gas where matrix (M) and fluid (F) particles interact via a smoothly truncated, purely repulsive Weeks-Chandler-Andersen (WCA) potential. The matrix structures are obtained as snapshots of high-temperature fluids at equilibrium (i.e., structural correlations in the matrix are very weak). The effective sizes of fluid and matrix particles according to the WCA interactions are given by σ_F and σ_M, respectively. Thus, the interaction range of the matrix with respect to the fluid particles is $\sigma_\mathrm{WCA} = (\sigma_\mathrm{M} + \sigma_\mathrm{F})/2$. One hundred statistically independent matrix structures with up to $N = 16000$ particles were generated. The number density is fixed to $n = N/L^2 = 0.278/\sigma_\mathrm{M}^2$, with $L/\sigma_\mathrm{M} = 240$ the linear dimension of the largest used system. Note that for a finite-size scaling analysis we also considered systems with smaller numbers of particles. Below, only the results for the largest systems are shown. For more details on the Lorentz model with WCA interactions and the simulations, we refer to references [30,33].

As a control parameter for the study of the delocalization-to-localization transition of this model, we use the reduced density $n^*_\mathrm{WCA} = n\sigma^2_\mathrm{WCA}$ which is tuned via the variation of the interaction range σ_WCA. Two cases are considered: (i) Systems where the fluid particles have the same energy (corresponding to a microcanonical ensemble). Here, the energy was numerically obtained from equilibration runs, where non-interacting tracers were inserted into the matrix and then equilibrated at

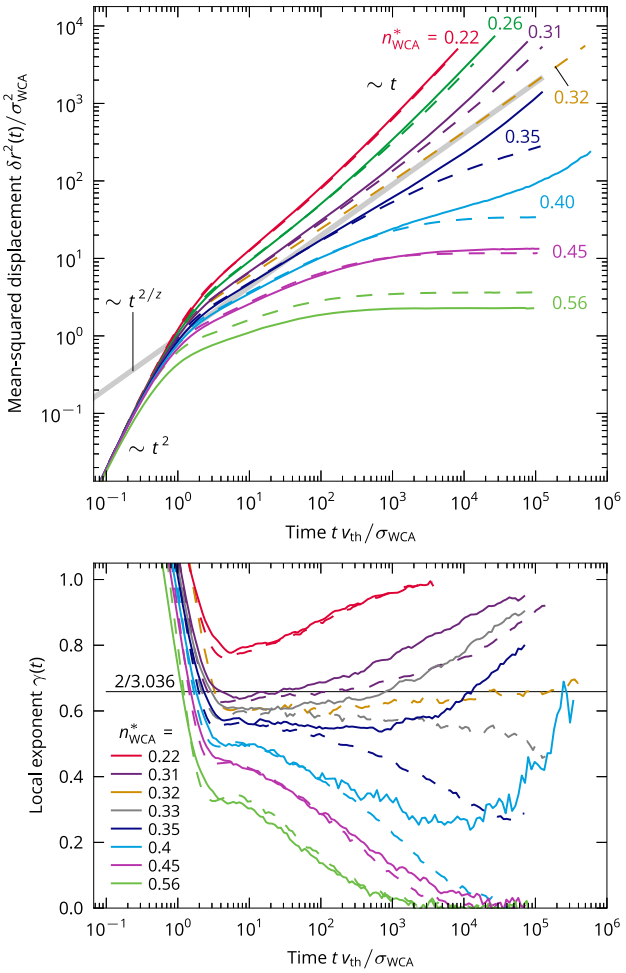

Fig. 1. Upper panel: MSDs of the WCA system for a canonical ensemble of tracers (solid lines) and tracers with single energy (dashed lines) for different values of n^*_{WCA}, as indicated. The straight line $\sim t^{2/z}$ with the dynamic exponent $z = 3.036$ of the Lorentz model serves as guide to the eye. Time t is scaled with the factor $v_{\mathrm{th}}/\sigma_{\mathrm{WCA}}$ where $v_{\mathrm{th}} = (k_B T/m)^{1/2}$ is the thermal velocity of the tracers (with $k_B T$ the thermal energy and m the mass). Lower panel: local exponent, $\gamma(t)$, calculated from the MSDs of the upper panel; again solid lines correspond to a canonical ensemble of tracers (solid lines) and dashed lines to the single-energy case. The horizontal line indicates the anomalous exponent $2/z$ with $z = 3.036$ of the Lorentz model. From reference [33].

temperature $k_{\mathrm{B}}T = 1$. The average energy per particle in these runs were then taken as the energy to be used in production runs. (ii) Systems in a canonical ensemble where the fluid particles have a distribution of energies. So we just took the equilibrated samples at temperature $k_{\mathrm{B}}T = 1$ as initial configurations for the production runs. Note that only the second case applies to the experimental setup, described in the previous section.

Figure 1a displays the MSDs for the fluid particles forming an ideal gas in the canonical ensemble (solid lines) and those having exactly the same energy (dashed lines). For $n^*_{\mathrm{WCA}} \leq 0.26$, the ideal gas and the single-energy system show a linear growth of the MSD at long times, indicating normal diffusion, and are in quantitative agreement with each other. This changes at higher densities. While at long times the

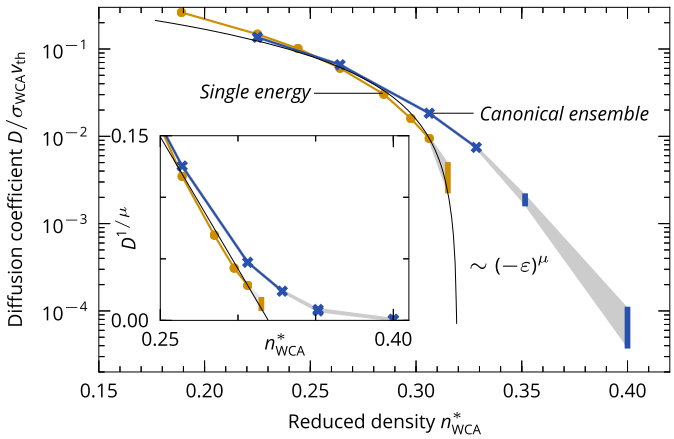

Fig. 2. Diffusion coefficient D of the WCA system for a canonical ensemble of tracers and the single-energy case as function of the reduced obstacle density n^*_{WCA}. Connected symbols are obtained directly from the mean-squared displacements, isolated errorbars at higher densities from finite-size scaling, see text. The solid black line $\propto (n^*_{\mathrm{WCA,crit}} - n^*_{\mathrm{WCA}})^{\mu}$ with the exponent $\mu = 1.309$ of the Lorentz model serves as guide to the eye. Inset: rectification plot of the same data. From reference [33].

MSD for the one-energy system shows the predicted power law with the exponent $2/3.036$ at $n^*_{\mathrm{WCA}} = 0.32$ over about three orders of magnitude in time, the ideal gas system becomes diffusive even at a density of $n^*_{\mathrm{WCA}} = 0.40$ and it never matches the critical subdiffusive behavior of the Lorentz model. However, for $n^*_{\mathrm{WCA}} > 0.4$ both systems are in a localized state, as indicated by the appearance of a plateau of the MSD in the long-time limit.

The differences between the two systems become even more evident from the inspection of the local exponent $\gamma(t)$ of the MSD in Figure 1b. The local exponent is defined by the following logarithmic derivative of the MSD with respect to time,

$$\gamma(t) = \frac{d\,\log(\delta r^2(t))}{d\,\log(t)}. \tag{1}$$

Figure 1b clearly indicates for both systems a transition from a delocalized state at low densities with $\gamma(t) = 1$ for $t \to \infty$ to a localized state at high densities with $\gamma(t) = 0$ for $t \to \infty$. However, only in the one-energy case the expected anomalous diffusion with $\gamma(t) = 2/3.036$ for $t \to \infty$ is seen at a critical density of about $n^*_{\mathrm{WCA,crit}} = 0.32$. In contrast to that, the ideal gas system exhibits a rounded transition around this critical density.

The difference between the two systems is also apparent in the long-time diffusion coefficient,

$$D = \lim_{t\to\infty} \frac{\delta r^2(t)}{4t}. \tag{2}$$

According to the prediction for the Lorentz gas, the diffusion coefficient vanishes with a power law in the vicinity of the critical density [34,35], $D \propto (n^*_{\mathrm{WCA,crit}} - n^*_{\mathrm{WCA}})^{\mu}$ for $n^*_{\mathrm{WCA}} \leq n^*_{\mathrm{WCA,crit}}$. In two dimensions, the prediction for the exponent is $\mu = 1.309$. While the single-energy system is consistent with the prediction for the Lorentz gas, the ideal gas system exhibits a finite diffusion coefficient at $n^*_{\mathrm{WCA,crit}}$ and a decay which is weaker than the predicted power law (Fig. 2). This is particularly evident from the rectification plot given in the inset of Figure 2.

The modified Lorentz model with WCA interactions only exhibits the critical dynamics of the original Lorentz model with hard interactions if one considers it in a microcanonical ensemble where all the tracer particles are set to the same energy. In the ideal gas case, the distribution of tracer particle energies leads to a rounding of the delocalization-to-localization transition. As shown in reference [33], one can assign to each tracer particle as a function of n^*_{WCA} and its energy E an effective hard-disk interaction diameter $\sigma_{\mathrm{eff}}(E)$. From this diameter, a reduced density can be defined, $n^*_{\mathrm{eff}}(E) = n\sigma^2_{\mathrm{eff}}$. Then, when one plots the diffusion coefficient as a function of n^*_{eff}, agreement with the single-energy case is obtained. This means that also in the ideal gas case each tracer particle can be fully mapped onto the Lorentz model as a function of its diameter and its energy.

The situation becomes more complicated in the case of interacting tracer particles. Here, due to the interaction between the tracer particles, each tracer particle samples the full energy distribution over time. Via collisions among each other, the tracer particles can help each other over barriers and therefore the void space is not static anymore as for the non-interacting tracer particles. As a consequence a rounding of the delocalization-to-localization transition is seen which surprisingly can be accompanied by the presence of nonlinear, subdiffusive regimes in the MSD over 3–4 orders of magnitude. However, the exponents for the subdiffusion in this case are non-universal and depend on the details of the interactions and the density of the fluid of tracer particles. More details on the soft-sphere Lorentz gas with interacting tracer particles can be found in references [36,37].

Particularly the results for the soft-sphere Lorentz gas with interacting tracer particles provide a challenge for mean-field-like approaches such as the mode coupling theory for pinned particle systems, as proposed by Krakoviack [17,18]. In the framework of such theories, the "dynamic arrangement" of barriers in the void space due to the interaction between tracer particles cannot be taken into account and thus there is always a sharp transition from a delocalized to a localized motion at a critical density.

3 Active non-linear micro-rheology in a glass-forming mixture

Active micro-rheology (AMR) can be seen as a tool to probe the mechanical response of bio- and soft matter systems on a local scale [5,38,39]. In a typical AMR experiment on colloidal systems, one pulls an individual tracer particle through the system with a constant external force f. In the steady state, the tracer has a constant velocity v and one can define a friction coefficient ξ via $\xi = f/v$. In the linear response regime, i.e., at sufficiently low forces, the friction coefficient is independent of f and directly related to the self-diffusion coefficient, D, of the tracer by a fluctuation-dissipation theorem, $D = k_B T/\xi$. Approaching the glass transition in glass-forming systems, the linear response regime shrinks to a window of very small forces and disappears at the glass transition [40]. Thus, AMR experiments and simulations on glass-forming fluids are associated with a strong non-linear response (see, e.g., Refs. [41–51]), as indicated – analogous to shear-thinning in macro-rheology – by a strong decrease of the friction coefficient as function of the force f. As we show in the following, the non-linear response in AMR is linked with anomalous diffusion dynamics.

To this end, we perform molecular dynamics simulation of a three-dimensional glass-forming binary AB Yukawa mixture [52,53]. This is an equimolar mixture at the number density $n = 0.675/d^3$ (with d the diameter of A particles). Note that the reduced critical mode coupling temperature of this model is at $T = 0.14$. Fully equilibrated configurations were generated in the temperature range, $1.0 \leq T \leq 0.14$, as well as configurations at $T = 0.1$ where the system is in a glass state. These

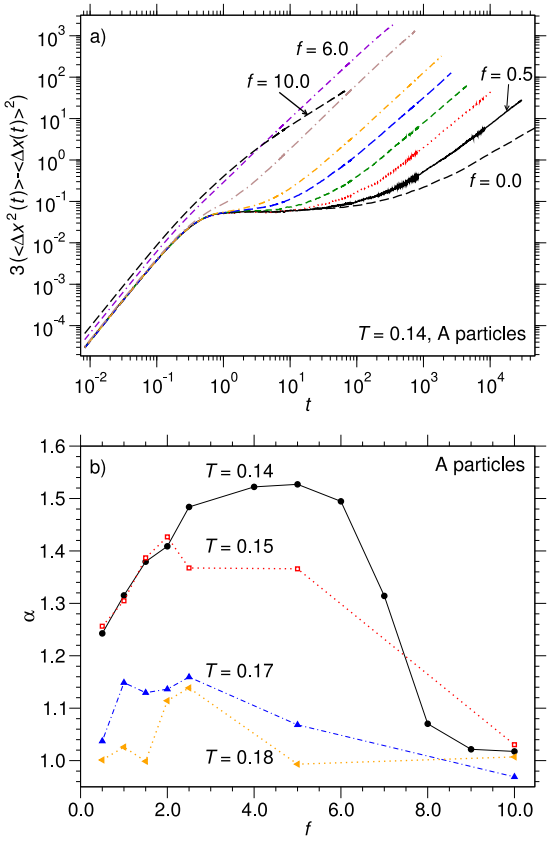

Fig. 3. (a) Mean-squared displacement $\langle \Delta x^2(t) \rangle - \langle \Delta x(t) \rangle^2$ for pulled A particle at $T = 0.14$. The curves correspond to the forces $f = 0.0$, 0.5, 1.0, 1.5, 2.5, 4.0, 6.0, and 10.0 (from right to left). Note that for $f \neq 0$, the MSDs are multiplied by a factor of 3 to allow for a direct comparison with the $f = 0$ case. (b) Effective exponents α as a function of f for different temperatures, as indicated. From reference [44].

configurations serve as initial configurations for the AMR runs where single particles are pulled with a constant external force $\mathbf{F} = (f, 0, 0)$ in x-direction, assuming periodic boundary conditions in all three spatial directions. The force f was varied in the range $5 \leq f \leq 30$, with f in units of $k_B T/d$. About 1000 independent trajectories of pulled particles were simulated at each force and temperature to obtain data with a reasonable statistics. A dissipative particle dynamics (DPD) thermostat is used to keep the temperature of the system constant [54]. More details on the Yukawa model and simulations can be found in reference [44].

Anomalous transport can be inferred from the drift-corrected MSD in x-direction, i.e., in force direction, which is defined by $\langle \Delta x^2(t) \rangle - \langle \Delta x(t) \rangle^2 = \langle (x(t) - x(0))^2 \rangle - \langle (x(t) - x(0)) \rangle^2$. Figure 3a shows this MSD for the A particles at the temperature $T = 0.14$ in the force range $0.0 \leq f \leq 10.0$. With increasing f, the dynamics becomes faster and qualitatively different from the $f = 0.0$ case; a superlinear behavior $\langle \Delta x^2(t) \rangle - \langle \Delta x(t) \rangle^2 \propto t^\alpha$ with $\alpha > 1$, is seen at long times and intermediate forces. This can be more clearly inferred from Figure 3b where the exponent α is plotted as function of f for different temperatures. At $T = 0.14$, it first increases from about 1.3 to 1.5 in the interval $0.5 \leq f \leq 2.5$, then it is constant around 1.5 between $f = 2.5$ and $f = 6$, before it decreases to 1.0 for $f > 6$. At higher temperatures the behavior

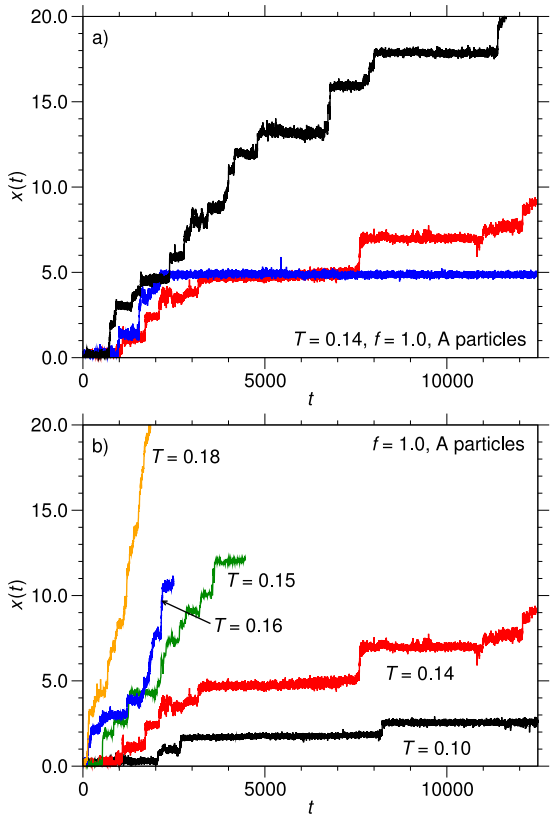

Fig. 4. (a) Typical trajectories, $x(t)$, of pulled A particles at $T = 0.14$ and $f = 1.0$. (b) Typical trajectories, $x(t)$, of pulled A particles at $f = 1.0$ and different temperatures, as indicated. From reference [44].

of α is qualitatively similar to this temperature, but the effective exponents are significantly lower than for $T = 0.14$. From this, we can conclude that the superlinear (or superdiffusive) behavior is directly related to the time scale separation between the motion of the pulled tracer particle and that of the surrounding host fluid. A pronounced superdiffusive behavior is seen if the surrounding host fluid is quasi-frozen on the time scale of the tracer particle. However, in the limit of very long times, i.e., on time scales where the particles of the host fluid exhibit a diffusive motion, one would expect a crossover to normal diffusion also for the tracer particle.

The time scale separation between the motion of the pulled tracer particle and the quasi-frozen host liquid is associated by a hopping motion of the tracer from cage to cage. This is indicated in Figure 4b which shows typical trajectories for the force $f = 1.0$. While at high temperatures, say at $T = 0.18$, the trajectory is relatively smooth, at low temperatures one can clearly identify the residence in the cage and the hop to the next cage. Furthermore, the residence time τ in the cages is rather heterogeneous at low temperatures (cf. the trajectories at $T = 0.14$ in Fig. 4a). In fact, waiting time distributions show broad tails towards large values of τ. Below we will see that a particle pulled through a two-dimensional random force field displays similar trajectories in force direction. Note also that for large forces the waiting time distribution does not exhibit any broad tails anymore and therefore, the diffusion in force direction becomes normal in this case [44,55], see Figure 3.

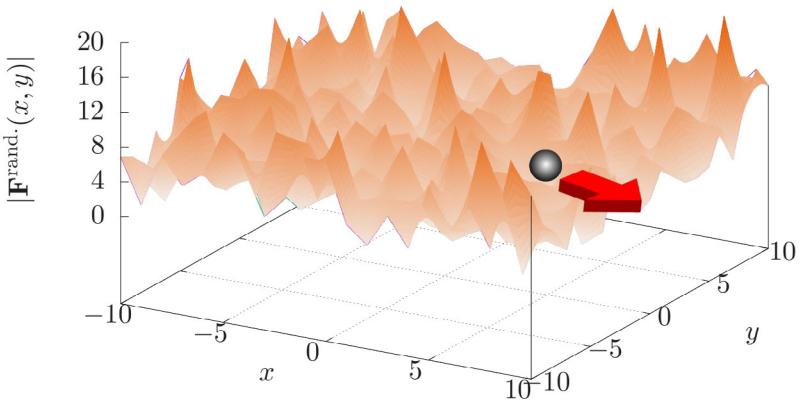

Fig. 5. Static random force field through which a particle is pulled with a constant force.

An interesting finding in references [42,44] concerns the dynamics of the pulled particle perpendicular to the force direction: One can bring the data for the friction coefficients of A particles at different temperatures and forces onto one master curve if one plots them as a function of an effective temperature, given by $T_{\text{eff}} = T + Cf^2$ (with C a constant). This also holds for the friction coefficients of B particles as well as the diffusion coefficients of A and B particles in the direction perpendicular to the force. However, in each case a different constant C is found [44]. We note that a similar f^2 dependence of the effective temperature is predicted in the framework of a mean-field theory for Brownian particles in the presence of a strong external force [56,57]. Further insight on the meaning of the effective temperature for AMR of glass-forming fluids in the framework of a potential energy landscape picture has been recently provided by Schroer and Heuer [47].

4 A particle pulled through a two-dimensional random force field

A simple model for a particle pulled through a random environment by a constant drift force F_{drag} has been introduced by Bouchaud et al. [9,10]. Here, a one-dimensional Langevin equation for a single particle in a spatially random force field $F_{\text{rand}}(x)$ is considered

$$\xi\dot{x} = F_{\text{rand}}(x) + \eta(t) + F_{\text{drag}}, \tag{3}$$

with x the position of the particle, ξ a friction coefficient, and $\eta(t)$ white noise with zero mean, $\langle\eta(t)\rangle = 0$, with respect to time t, and delta correlations $\langle\eta(t)\eta(t')\rangle = 2k_{\text{B}}T\delta(t-t')$ for different times t and t'. The random force field $F_{\text{rand}}(x)$ is spatially delta-correlated as

$$\langle F_{\text{rand}}(x)F_{\text{rand}}(x')\rangle = \sigma\delta(x-x'). \tag{4}$$

In the following, we refer to the model, defined by equations (3) and (4) as the Bouchaud model.

The diffusion dynamics of the Bouchaud model can be described in terms of one control parameter which is given by

$$\mu = \frac{2D_0F_{\text{drag}}}{\sigma}, \tag{5}$$

with $D_0 = k_{\text{B}}T/\xi$ the diffusion coefficient of the particle in absence of the random force field and the pulling force.

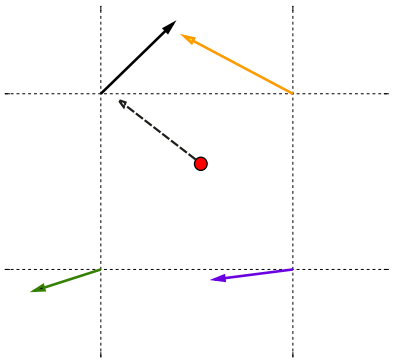

Fig. 6. Sketch that shows how the force on the tracer particle due to the quenched random force field is computed.

In the long-time limit, the Bouchaud model can be mapped onto a directed walk among traps with a broad release time distribution, given by a master equation for a one-dimensional lattice model with a random distribution of asymmetric transition rates at each lattice site. A remarkable feature of the Bouchaud model is a regime of asymptotic superdiffusion in the parameter range $1 \leq \mu \leq 2$, correponding to a regime where the drag force of the walker is sufficiently large such that the walker sees only very high potential barriers that are associated with the tails of the release time distribution.

It is tempting to consider the Bouchaud model as a minimal model for the occurrence of superdiffusion in connection with the driven transport through heterogeneous media. However, one has to keep in mind that up to now the Bouchaud model has only been solved in one dimension and in particular the appearance of superdiffusion might be a special feature of a driven system in one dimension. Therefore, here we extend the Bouchaud model to two dimensions and investigate the diffusion dynamics of this model numerically.

Thus, we solve the two-dimensional version of equations (3) and (4) in terms of a Brownian dynamics simulation. To this end, equation (3) is integrated using a first-order Euler algorithm with time step $\delta t = 10^{-3}$. The thermal energy $k_{\mathrm{B}}T$ and the friction coefficient ξ are set to unity. To implement the quenched random force field, the system is divided into a square regular grid of size 1 and at each grid point (i, j) a random force $F_{\mathrm{rand}}(i, j)$ is assigned via a uniformly distributed random number. Then, at each time step we identify in which cell of the above mentioned lattice the particle is located; the force exerted on that particle is calculated by a (bi-linear) interpolation of the four force values on the corners of that cell (see Fig. 6).

As in the one-dimensional case, the transport properties of the two-dimensional model are controlled by one parameter μ, see equation (5). The characteristic length scale of the system is $x_0 = 4D_0^2/\sigma$ and the time scale is $t_0 = x_0^2/4D_0$. All the results presented below are given in units of x_0 and t_0.

To analyze the diffusion dynamics in force direction (x-direction), we compute the mean-squared displacement in x direction and subtract the drift motion. So as in the previous Section for AMR, we define

$$\mathrm{Var}_x = \langle (x(t) - x(0))^2 \rangle - (\langle (x(t) - x(0)) \rangle)^2 \,. \tag{6}$$

This quantity and the corresponding local exponent $\gamma(t)$, as defined by equation (1), are plotted in Figure 7 for different values of μ. Note that at short times Var_x grows linearly with time since we now consider overdamped Brownian dynamics and not Newtonian dynamics as in the case of AMR in the previous chapter. At $\mu = 0$, normal

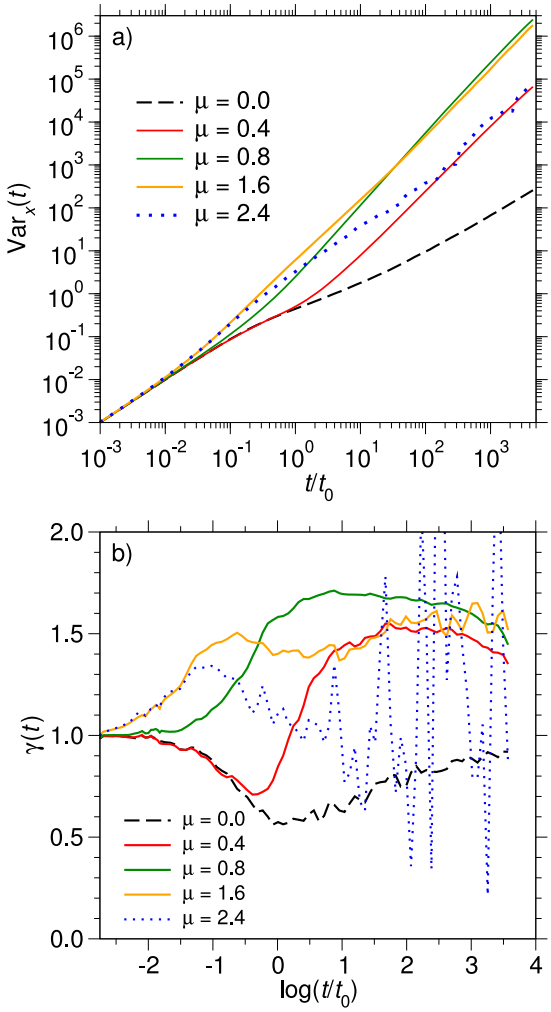

Fig. 7. (a) Var_x and (b) the corresponding local exponent $\gamma(t)$, see equation (1), for different values of μ.

diffusion is obtained at long times, preceeded by a subdiffusive regime at intermediate times. For finite values of μ, a superdiffusive regime can be inferred at intermediate times which might even control the long-time behavior for $\mu > 1$, as in the one-dimensional Bouchaud model. However, here our simulation results are preliminary and not conclusive yet. Longer runs are required the results of which will be presented in forthcoming studies. Nevertheless, similar to the one-dimensional Bouchaud mode for $\mu > 2$ the dynamics becomes diffusive again.

Although in our simulations F_{drag} is aligned with the x-direction, it affects the transport along the y-direction in a non-trivial manner. Figure 8 shows the mean-squared displacement in y-direction, $\delta y^2(t) = \langle (y(t) - y(0))^2 \rangle$, as well as the corresponding $\gamma(t)$. Although for all values of μ, $\delta y^2(t)$ increases linearly in the long-time limit, it also exhibits a superlinear regime at intermediate times. While we do not yet understand this feature, we would like to mention that a similar behavior has been also recently observed in a lattice model of a pulled tracer particle in the presence

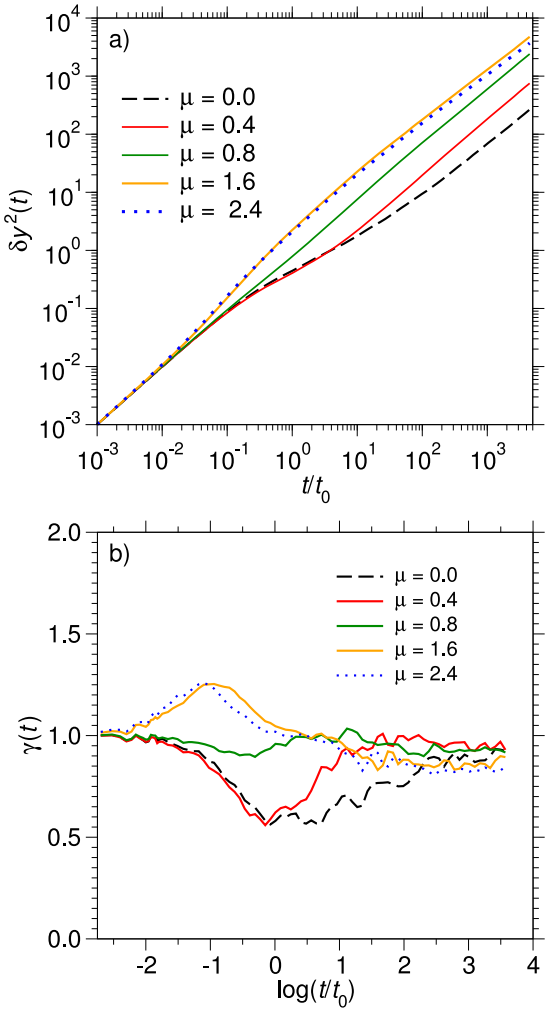

Fig. 8. (a) Mean-squared displacement in y-direction, $\delta y^2(t)$ and (b) the corresponding local exponent $\gamma(t)$ for different values of μ.

of obstacles [58]. Note that a superlinear regime in the direction orthogonal to the driving is not seen for the AMR of glassforming fluids.

Figure 9 shows different trajectories in force direction for different values of μ. Especially at $\mu = 0.4$ the trajectories look similar to those found in the AMR of the binary Yukawa mixture (cf. Fig. 4). Fast hops from one minimum in the random force landscape to the next minimum can be interrupted by long residence times in a minimum. The trajectories also indicate that the distribution of these residence times, $P(\tau)$, is very heterogeneous and one expects the occurrence of broad tails in $P(\tau)$ for large residence times τ, as in the case of the aforementioned AMR. The analysis of residence time distributions is the subject of forthcoming studies. Such an analysis is the key for the understanding of the superdiffusive behavior in both Var_x and δy^2 and will also clarify whether there are ranges of μ values where the superlinear increase of Var_x is seen in the long-time limit.

More information about the dynamics of the pulled tracer particle in the random force landscape can be obtained from the van Hove correlation functions (displacement

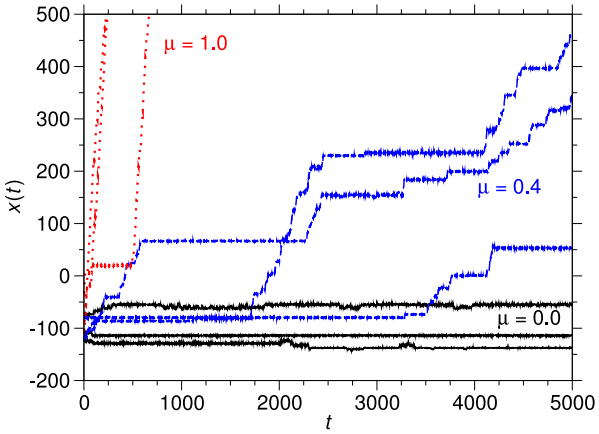

Fig. 9. The trajectory of a particle which is pulled in the system. The pulling direction is from left to right but as the particle gets trapped, its motion along the neutral direction is also impeded.

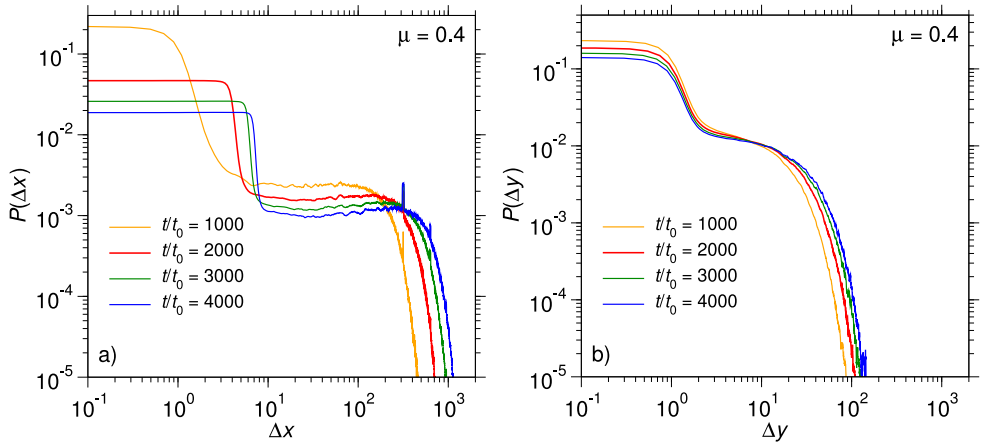

Fig. 10. The displacement distributions $P(\Delta x)$ and $P(\Delta y)$ for $\mu = 0.4$ and different times in the long-time regime are shown in (a) and (b), respectively.

distribution functions) in both directions, $P(\Delta x)$ and $P(\Delta y)$. Here, the displacements in x and y direction are given by $\Delta x = x(t) - x(0)$ and $\Delta y = y(t) - y(0)$, respectively. The functions $P(\Delta x)$ and $P(\Delta y)$ are displayed in Figure 10 for $\mu = 0.4$ and several times for $t \geq 10^3$, which corresponds to the long-time regime with superdiffusive behavior in x-direction. It is remarkable that although the distributions in Figure 10 correspond to the long-time regime, they indicate a significant fraction of particles that have only moved over short distances and they are still trapped in a minimum in the random force landscape in which they have already been at time $t = 0$. Other particles have meanwhile moved over large distances (note the logarithmic x axis in Fig. 10). This also reflects the broad distribution of residence times in traps, which could explain the superdiffusive behavior.

Superdiffusion has also been observed in other model systems, considering the driven transport of single particles through a heterogeneous medium. Recently, Leitmann and Franosch [58] presented an analytical calculation (combined with computer simulations) of a tracer particle on a lattice pulled by a constant force in the presence of immobile obstacles. For the variance in force direction, Var_x, they find

superdiffusive regimes on intermediate time scales that become more pronounced with increasing pulling force. In a different lattice model proposed by Bénichou et al. [59] superdiffusion of driven tracer particles in the long-time limit is induced by geometrical confinement.

It would be nice to realize simple driven model systems also experimentally. For colloidal systems, light fields can be used to generate two-dimensional random-energy landscapes [60,61]. However, it is an open question how these light fields could be used to obtain a random force field. This is also a subject of forthcoming studies.

5 Summary

In this review, we have studied anomalous transport phenomena that occur with respect to the single-particle dynamics in heterogeneous media. Three different cases have been considered: (1) two-dimensional fluids diffusing through a medium of randomly pinned particles, (2) active micro-rheology in a three-dimensional glass-forming binary mixture, and (3) a simple model for a particle pulled through a two-dimensional random force field. A central question that we addressed in this review was whether the anomalous transport in these systems is apparent as an effective feature on intermediate time scales or as a universal behavior that is seen asymptotically in the long time limit. In all three cases, non-universal behavior seems to dominate the diffusion dynamics in the long-time limit. However, the phenomena that we see can be only understood with reference to simple minimal models that exhibit universality.

We acknowledge the DFG research unit FOR 1394 (project P8, HO 2231/7) for funding. We thank Pinaki Chaudhuri, Roel Dullens, Stefan Egelhaaf, Thomas Franosch, Matthias Fuchs, Felix Höfling, Thomas Skinner, Markus Spanner, Alice Thorneywork, Thomas Voigtmann, and David Winter for fruitful collaborations in the framework of the FOR 1394 and Andreas Heuer and Vincent Krakoviack for very useful discussions on the topics of this work.

References

1. M.J. Saxton, Biophys. J. **103**, 2411 (2012)
2. I.M. Sokolov, Soft Matter **8**, 9043 (2012)
3. F. Höfling, T. Franosch, Rep. Prog. Phys. **76**, 046602 (2013)
4. P. Adler, *Porous Media: Geometry and Transport* (Butterworth-Heinemann, Stoneham, 1992)
5. T.M. Squires, T.G. Mason, Ann. Rev. Fluid Mech. **42**, 413 (2010)
6. P.C. Hohenberg, B.I. Halperin, Rev. Mod. Phys. **49**, 435 (1977)
7. W. Götze, *Complex Dynamics of Glass-Forming Liquids: A Mode-Coupling Theory* (Oxford University Press, Oxford, 2008)
8. H. Lorentz, Proc. R. Acad. Sci. Amsterdam **7**, 438 (1905)
9. J.P. Bouchaud, A. Comtet, A. Georges, P. Le Doussal, Ann. Phys. **201**, 285 (1990)
10. J.P. Bouchaud, A. Georges, Phys. Rep. **195**, 127 (1990)
11. A. Cavagna, T.S. Grigera, P. Verrocchio, J. Stat. Mech. **2010**, P10001 (2010)
12. C. Cammarota, G. Biroli, Proc. Natl. Acad. Sci. USA **109**, 8850 (2012)
13. C. Cammarota, G. Biroli, J. Chem. Phys. **138**, 12 A547 (2013)
14. L. Berthier, W. Kob, Phys. Rev. E **85**, 011102 (2012)
15. M. Ozawa, W. Kob, A. Ikeda, K. Miyazaki, Proc. Natl. Acad. Sci. USA **112**, 6914 (2015)
16. S. Chakrabarty, R. Das, S. Karmakar, C. Dasgupta, J. Chem. Phys. **145**, 034507 (2016)
17. V. Krakoviack, Phys. Rev. E **82**, 061501 (2010)
18. V. Krakoviack, J. Chem. Phys. **141**, 104504 (2014)
19. R. Benjamin, J. Horbach, Phys. Rev. E **90**, 060101(R) (2014)
20. W. Götze, E. Leutheusser, S. Yip, Phys. Rev. A **23**, 2634 (1981)

21. W. Götze, E. Leutheusser, S. Yip, Phys. Rev. A **24**, 1008 (1981)
22. W. Götze, E. Leutheusser, S. Yip, Phys. Rev. A **25**, 533 (1982)
23. E. Leutheusser, Phys. Rev. A **28**, 1762 (1983)
24. V. Krakoviack, Phys. Rev. E **79**, 061501 (2009)
25. V. Krakoviack, Phys. Rev. E **84**, 050501(R) (2011)
26. A.L. Thorneywork, R. Roth, D.G.A.L. Aarts, R.P.A. Dullens, J. Chem. Phys. **140**, 161106 (2014)
27. A.L. Thorneywork, R.E. Rozas, R.P.A. Dullens, J. Horbach, Phys. Rev. Lett. **115**, 268301 (2015)
28. A.L. Thorneywork, D.G.A.L. Aarts, J. Horbach, R.P.A. Dullens, Soft Matter **12**, 4129 (2016)
29. A.L. Thorneywork, D.G.A.L. Aarts, J. Horbach, R.P.A. Dullens, Phys. Rev. E **95**, 012614 (2017)
30. T.O.E. Skinner, S.K. Schnyder, D.G.A.L. Aarts, J. Horbach, R.P.A. Dullens, Phys. Rev. Lett. **111**, 128301 (2013)
31. S.K. Schnyder, T.O.E. Skinner, A.L. Thorneywork, D.G.A.L. Aarts, J. Horbach, R.P.A. Dullens, Phys. Rev. E **95**, 032602 (2017)
32. T. Bauer, F. Höfling, T. Munk, E. Frey, T. Franosch, Eur. Phys. J. Special Topics **189**, 103 (2010)
33. S.K. Schnyder, M. Spanner, F. Höfling, T. Franosch, J. Horbach, Soft Matter **11**, 701 (2015)
34. Y. Gefen, A. Aharony, S. Alexander, Phys. Rev. Lett. **50**, 77 (1983)
35. D. Ben-Avraham, S. Havlin, *Diffusion and Reactions in Fractals and Disordered Systems* (Cambridge University Press, Cambridge, 2000)
36. S.K. Schnyder, *Anomalous Transport in Heterogeneous Media*, Ph.D. thesis, Düsseldorf, 2014
37. S.K. Schnyder, J. Horbach, Unpublished
38. L.G. Wilson, W.C.K. Poon, Phys. Chem. Chem. Phys. **13**, 10617 (2011)
39. A.M. Puertas, T. Voigtmann, J. Phys.: Condens. Matter **26**, 243101 (2014)
40. S.R. Williams, D.J. Evans, Phys. Rev. Lett. **96**, 015701 (2006)
41. P. Habdas, D. Schaar, A.C. Levitt, E.R. Weeks, Europhys. Lett. **67**, 477 (2004)
42. D. Winter, J. Horbach, P. Virnau, K. Binder, Phys. Rev. Lett. **108**, 028303 (2012)
43. C.J. Harrer, D. Winter, J. Horbach, M. Fuchs, T. Voigtmann, J. Phys.: Condens. Matter **24**, 464105 (2012)
44. D. Winter, J. Horbach, J. Chem. Phys. **138**, 12 A512 (2013)
45. C.F.E. Schroer, A. Heuer, Phys. Rev. Lett. **110**, 067801 (2013)
46. C.F.E. Schroer, A. Heuer, J. Chem. Phys. **138**, 12 A518 (2013)
47. C.F.E. Schroer, A. Heuer, J. Chem. Phys. **143**, 224501 (2015)
48. R. Wulfert, U. Seifert, T. Speck, Phys. Rev. E **94**, 062610 (2016)
49. A. Fiege, M. Grob, A. Zippelius, Granular Matter **14**, 247 (2012)
50. T. Wang, M. Grob, A. Zippelius, M. Sperl, Phys. Rev. E **89**, 042209 (2014)
51. T. Wang, M. Sperl, Phys. Rev. E **93**, 022606 (2016)
52. J. Zausch, J. Horbach, M. Laurati, S.U. Egelhaaf, J.M. Brader, T. Voigtmann, M. Fuchs, J. Phys.: Condens. Matter **20**, 404210 (2008)
53. J. Zausch, J. Horbach, EPL **88**, 60001 (2009)
54. E.A.J.F. Peters, Europhys. Lett. **66**, 311 (2004)
55. R.L. Jack, D. Kelsey, J.P. Garrahan, D. Chandler, Phys. Rev. E **78**, 011506 (2008)
56. I. Santamaria-Holek, A. Perez-Madrid, J. Phys. Chem. B **115**, 9439 (2011)
57. I. Santamaria-Holek, A. Perez-Madrid, J. Chem. Phys. **145**, 134905 (2016)
58. S. Leitmann, T. Franosch, Phys. Rev. Lett. **118**, 018001 (2017)
59. O. Bénichou, A. Bodrova, D. Chakraborty, P. Illien, A. Law, C. Mejía-Monasterio, G. Oshanin, R. Voituriez, Phys. Rev. Lett. **111**, 260601 (2013)
60. F. Evers, C. Zunke, R.D.L. Hanes, J. Bewerunge, I. Ladadwa, A. Heuer, S.U. Egelhaaf, Phys. Rev. E **88**, 022125 (2013)
61. R.D.L. Hanes, S.U. Egelhaaf, J. Phys.: Condens. Matter **24**, 464116 (2012)